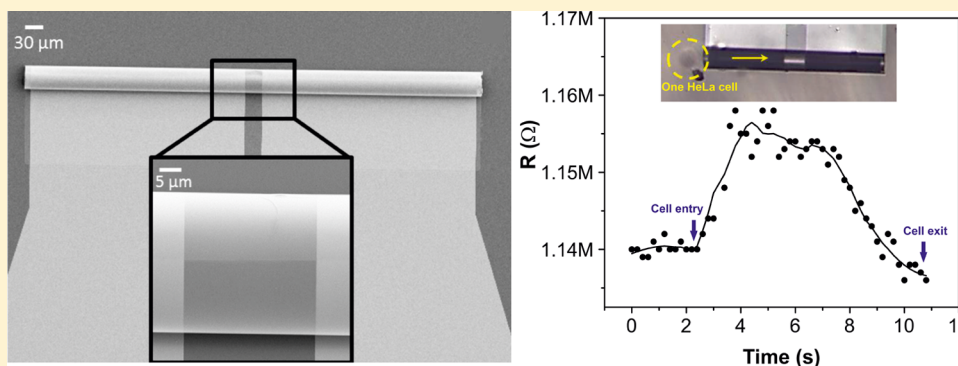


# Ultracompact Three-Dimensional Tubular Conductivity Microsensors for Ionic and Biosensing Applications

Cynthia S. Martinez-Cisneros,\* Samuel Sanchez,\* Wang Xi, and Oliver G. Schmidt\*

Institute for Integrative Nanosciences, IFW Dresden, Helmholtzstrasse 20, 01069 Dresden, Germany

**S** Supporting Information



**ABSTRACT:** We present ultracompact three-dimensional tubular structures integrating Au-based electrodes as impedimetric microsensors for the in-flow determination of mono- and divalent ionic species and HeLa cells. The microsensors show an improved performance of 2 orders of magnitude (limit of detection = 0.1 nM for KCl) compared to conventional planar conductivity detection systems integrated in microfluidic platforms and the capability to detect single HeLa cells in flowing phosphate buffered saline. These highly integrated conductivity tubular sensors thus open new possibilities for lab-in-a-tube devices for bioapplications such as biosensing and bioelectronics.

**KEYWORDS:** Rolled-up electronics, 3D-microsensor, lab-in-a-tube, nanomembranes

The recent interest on highly integrated microanalytical devices has promoted the development of hybrid fabrication technologies that enable the miniaturization and integration of all the stages associated to a (bio)analytical procedure in a single device. The development of microfluidic platforms for environmental, (bio)chemical and, more recently, cellular biology applications, has presented an exponential growth in the last decades.<sup>1–6</sup> Silicon, glass, polymers, and ceramics are usually the materials of choice for the attainment of accurate structures that may integrate some steps of a classical analytical procedure (sampling, separation, digestion, detection, and so forth) toward lab-in-a-chip devices.<sup>6–11</sup> Electrochemical detection,<sup>12–14</sup> especially conductivity detection, offers great potentiality for microfluidic platforms with features including high sensitivity, excellent miniaturization capability, low-power requirements, compatibility with advanced microfabrication technologies, relative low cost, and a high potential for portability.<sup>15</sup> Miniaturization of the detection electrodes could even result in an improved sensitivity as a result of the reduced noise.<sup>16</sup> By applying alternating current between electrodes, conductance changes can be measured in solutions of varied ionic species, a well-established and “label-free” detection technique.<sup>17</sup> The conductivity ( $\kappa$ ) of an electrolyte ( $E$ ) is given by the molar conductivity ( $\lambda$ ) of the ionic species ( $E^+$  and  $E^-$ ) and their concentrations ( $c$ ), according to the equation<sup>18</sup>

$$\kappa = \lambda_{E^+} \cdot c_{E^+} + \lambda_{E^-} \cdot c_{E^-} \quad (1)$$

Several efforts have been put toward the integration of conductivity detectors in microfluidic platforms.<sup>19,20</sup> Nevertheless, due to technological limitations in the main microfabrication technologies available today, the integration of geometries equivalent to in-flow conventional devices at the macroscale, where electrodes are in a tubular configuration around the channel, is very challenging and thus not reported so far. Therefore, planar electrodes, which are much easier to be integrated into chips, are nearly the only geometry found in the literature.<sup>17,21</sup> There are generally three electrode configurations: embedded in the microchip, attached to it (placed either underneath the bottom or on top of the device), or external to the device.<sup>21</sup> One limitation of such devices is the reduced sensitivity. To overcome this issue, some alternatives consist of increasing the detection area, decreasing the dielectric constant of the material, and minimizing stray capacitances. To increase the sensing area, configurations based on sidewall electrodes, semicircular and dual top-bottom have been proposed. Lee et al.<sup>22</sup> reported the construction of semicircular electrodes based on the deposition of Cr/Au around the

**Received:** March 2, 2014

**Revised:** March 18, 2014

**Published:** March 21, 2014

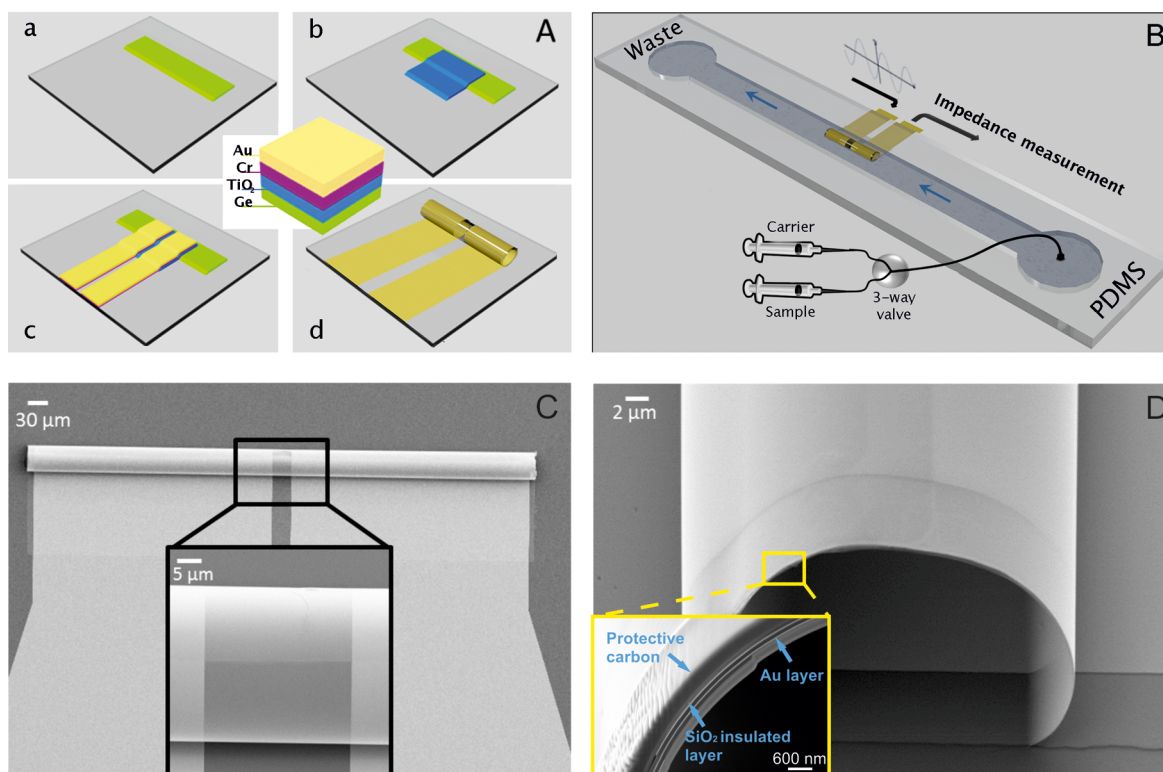


**Figure 1.** Fabrication process for 3D tubular microsensors. (A) Sequence of the layers deposition patterned by standard 2D photolithography and the rolling up of the nanomembranes: (a) 20 nm Ge sacrificial layer in green; (b) 60 nm TiO<sub>2</sub> layer in blue; (c) 5 nm Cr layer for enhancing gold adhesion in purple and 10 nm Au electrodes on top of the planar structure in yellow; and (d) rolling up the nanomembranes into rolled-up sensor after the selective etching of Ge in water. (B) A 3D schematic representation of the experimental setup for in-flow sensing. (C) SEM image of the 3D tubular microsensors 250 μm in length; the transparency of the strain layer enables to see the inner of the microtube and layers overlapping caused by the half extra winding. (D) Closed-up lateral view of the tubular structure with an outer diameter of 30 μm. Inset in D presents a FIB cut performed to the microtube to observe its cross section. There, one can observe the Au electrodes on the TiO<sub>2</sub> surface, leading to a tubular structure with inner electrodes which will be in direct contact with the solution flowing through the tube. The additional external and internal layers observed correspond to the protective carbon layer and the waste generated during the cut, respectively.

channel, demonstrating an increased sensitivity when compared with planar configurations. Following that approach, Mahabadi et al.<sup>23</sup> described a dual top–bottom electrochemical cell configuration, which consists of two pairs of copper strips embedded into two polymer blocks placed inside the housing at the top and the bottom. The authors claim that by increasing the detection area, the total capacitance increases and enable an enhancement on the signal coupling with the detection volume of the sample, leading to a signal increase from 40 to 65% in terms of peak height when compared to conventional top–top electrode geometry. Thus, to further increase the detection area and, consequently, the signal coupling and sensitivity of a detection system integrated to microfluidic platforms, one possibility is to recreate tubular electrodes as microfluidic channels with the inner/outer wall functioning as sensing area. This is a challenge affordable using the self-assembled rolled-up technology. Such self-assembled devices rely on differentially strained oxide, metallic, or semiconductor layers that roll-up into a tubular geometry once released from a host substrate by selective etching of a sacrificial layer underneath.<sup>24–26</sup> Self-assembled rolled-up structures have become very attractive in several application fields,<sup>27</sup> which include micro/nano fluidics,<sup>27,28</sup> microrobotics,<sup>29,30</sup> optics,<sup>31,32</sup> micro/nano electronics,<sup>33,34</sup> magnetic,<sup>28,35</sup> and chemical sensors<sup>36</sup> as well as energy storage.<sup>37,38</sup> In particular, single cells have previously been detected optically in a flexible split-wall microtube

resonator sensor.<sup>39</sup> The great versatility of the conductive patterns that can be embedded in/out of the tubular structure and their three-dimensionality enable the definition of tubular microchannels for label free sensing applications.

In this work, a hybrid self-assembled rolled-up tubular structure with microelectrodes embedded on its inner surface was fabricated and integrated in a PDMS-based microchip toward a lab-in-a-tube device for electrochemical measurements. The axial configuration of the sensor enables to overcome the main limitation regarding microfluidic structures, that is, the use of planar electrodes. The self-rolling process used for the development of the three-dimensional (3D) tubular microsensors is outlined in Figure 1A. It starts with the fabrication of a planar strained multilayer nanomembrane by the sequential deposition of oxide and metallic thin films on the surface of a sacrificial layer. In this case, the strained multilayer nanomembrane consists of a 60 nm TiO<sub>2</sub> thin film deposited on top of a sacrificial layer of 20 nm Ge. The electrodes consist of 5 nm of Cr followed by 10 nm of Au patterned by conventional photolithography on top of the TiO<sub>2</sub> surface. The strained multilayer nanomembranes rolled-up into microtubes with electrodes inside by the selective etching of the underlying Ge layers using water as solvent (Figure 1B). This rolling-up methodology based on water makes the device compatible for further bioapplications, including biofunctionalization of electrodes/surfaces, cytometry, cell sorting/manipulation and

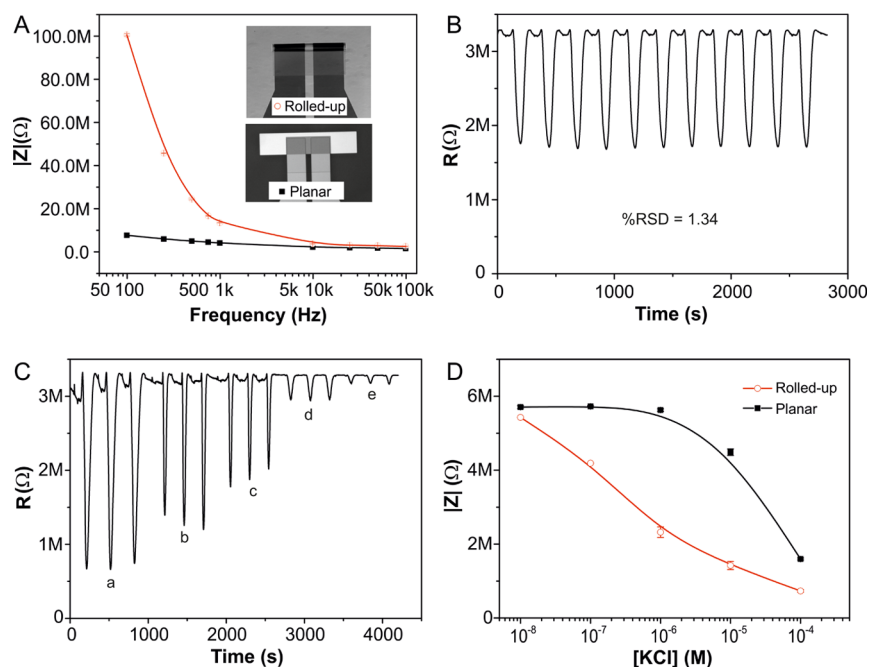


**Figure 2.** (A) Frequency dependence of the impedance of the 3D tubular microsensor and its equivalent planar configuration. (B) Sequential injections of KCl 0.1 mM to test the stability of the 3D tubular microsensor. The % RSD was found to be 1.34% ( $n = 11$ ; at 95% confidence). (C) Calibration performed with the 3D tubular microsensor for several KCl concentrations: [a] =  $10^{-4}$  M; [b] =  $10^{-5}$  M; [c] =  $10^{-6}$  M; [d] =  $10^{-7}$  M; and [e] =  $10^{-8}$  M. (D) Calibration plots obtained for KCl at different concentrations ( $10^{-4}$ – $10^{-8}$  M) for sensors in planar or 3D tubular configuration. Higher sensitivity can be clearly observed in the axial tubular sensor when compared to its thin-film planar counterpart when KCl concentration is lower than  $10^{-6}$  M.

biosensing, among others. Rather than photoresist, the use of Ge, which is etched slowly by water, leads to more compact and stable tubular structures during the rolling process.<sup>34</sup> This stability avoids some additional dehydration treatments and enables the repeated use of the devices. After rolling up, a 250  $\mu\text{m}$  long compact tubular architecture with 1.5 windings and an outer diameter of 30  $\mu\text{m}$  was obtained (see scanning electron microscopy (SEM) images in Figures 1C and 1D). The tubular electrodes inside the tube were 30  $\mu\text{m}$  longitudinally separated along the  $\text{TiO}_2$  inner surface, defining a tubular detection volume of 169  $\mu\text{L}$ .<sup>40</sup> The transparency of the  $\text{TiO}_2$ , inset in Figure 1C, would enable the simultaneous optical detection and observation of bio-organisms and labeled molecules flowing through the microtube. This is of special interest for applications in the field of cellular biology, because cells can be monitored both electrically and optically.

To further improve the mechanical stability and the sensitivity of the 3D electrodes configuration, we isolated the exposed area of the electrodes (outside of the microtube) by depositing 100 nm of  $\text{SiO}_2$ . In this way, only the electrodes defined in the inner surface of the microtubes were in direct contact with the analyte (ionic solution/cells). We tested the 3D tubular approach in continuous flow conditions, using the experimental setup presented in Figure 1B. The tubular microsensor was then integrated into a polydimethylsiloxane (PDMS)-based microfluidic device fabricated using standard soft lithography.

A planar microsensor containing the same strained multilayer nanomembranes was used as control during the impedance measurement (Figure 2A insets for comparison). Figure 2A shows Bode plots for planar (black squares) and tubular (red circles) microsenors flowing aqueous solutions containing KCl  $10^{-4}$  M as analyte. Flow rate and sample volume were set at 18

$\mu\text{L}/\text{min}$  and 20  $\mu\text{L}$ , respectively. The procedure was performed at three different potentials (0.5, 1, and 2 Vpp). We observed no significant difference when different potentials were applied, thus for later experiments we used 1 Vpp. Error bars were calculated from triplicate of signals at each frequency and potential, showing a highly repeatable system. At low frequencies, the impedance is limited by the double layer capacitances. For higher frequencies, the impedance depends only on the resistance of the solution, resulting in a plateau. It is important to operate the sensor at a frequency in the plateau region for maximum signal strength and to avoid peak distortions, which occur at lower frequencies.<sup>41,42</sup> We observed a higher sensitivity to frequency in the rolled-up configuration at the lower frequencies region (below 10 kHz). In traditional microfluidic chips, the use of dual top-bottom electrode geometries, doubles the total capacitance and enables an enhancement on the signal coupling with the sample volume when compared with top-top planar geometries.<sup>21</sup> Therefore, an increase of the total capacitive effect of the rolled-up system, caused by the use of an axial sensor instead of a planar one, would be expected, and is illustrated in Figure 2A.

Figure 2B demonstrates the repeatability and stability of the electrochemical system, which was estimated as the relative standard deviation (RSD), for a concentration of 0.1 mM KCl, RSD = 1.34% ( $n = 11$ ; at 95% confidence). The limit of detection (LOD) was calculated as three times the standard deviation of the baseline signal, which resulted in a value of 0.1 nM, 2 orders of magnitude lower when compared to similar in-flow conductivity sensors reported in the literature.<sup>19</sup>

To test the analytical response of the 3D tubular microsensor, we performed a calibration using KCl as a model analyte at concentrations ranging from  $10^{-8}$  M to  $10^{-4}$  M, using the same experimental conditions as previously. The impedance

measurements were done by applying a sinusoidal signal 1 V<sub>pp</sub> with a frequency of 50 kHz, which is in the plateau region of the frequency response graph previously obtained in Figure 2A. Figure 2C presents the real-time resistance variations on the 3D tubular microsensor when triplicate injections of KCl at different concentrations are performed. The magnitude of the impedance was estimated by using the expression  $|Z| = [R^2 + X^2]^{1/2}$ ; where  $R$  is resistance and  $X$  is reactance. The equation that describes the behavior of the system for KCl is

$$Y = -1.230E^{+6} (\pm 0.039E^{+6}) \cdot [\text{KCl}] - 4.410E^{+6} (\pm 0.315E^{+6})$$

$r^2 = 0.9701$  ( $n = 3$ ; 95% confidence). Figure 2D shows the calibration plots obtained for KCl at concentrations ranging from  $10^{-8}$  M to  $10^{-4}$  M using the rolled-up sample as well as the planar one under the same experimental conditions. According to these results, the 3D tubular microsensor presents a higher sensitivity when compared to its planar counterpart, which was not able to provide a significant difference on the signal response for concentrations below  $10^{-6}$  M. The planar device presented a linear behavior in the range from  $10^{-4}$  to  $10^{-6}$  M, which can be described by the expression

$$Y = -2.02E^{+6} (\pm 0.01E^{+6}) \cdot [\text{KCl}] - 6.18E^{+6} (\pm 0.08E^{+6})$$

$r^2 = 0.9402$  ( $n = 3$ ; 95% confidence). In this case the LOD was found to be  $0.8 \mu\text{M}$ .

The microfluidics-based setup enables to flow aqueous solutions containing different electrolytes through the 3D tubular microsensor in sequence and detect the ionic concentration. As cations, especially calcium ions, have been recognized as essential mediator in important physiological processes, such as cell proliferation and tumorigenesis,<sup>43,44</sup> our sensor then opens a fast, fully integrated and label-free way to detect cations with biorelevant interest at extremely low concentration. Figure 3A,B presents the real-time monitoring of the impedance while aqueous  $\text{NH}_4\text{Cl}$  and  $\text{CaCl}_2$  at concentrations ranging from  $10^{-3}$  to  $10^{-7}$  M flew through the microfluidic device. In this case, as for KCl, we performed a previous optimization procedure for each electroanalyte, including electrical and fluidic parameters, in order to obtain the highest sensitivity for each of them. The insets in Figure 3 show the calibration plot obtained for each salt. The limit of detection (LOD) was calculated as three times the standard deviation of the base signal, resulting in values of 87 nM for  $\text{NH}_4\text{Cl}$  and 100 nM for  $\text{CaCl}_2$ , respectively. These data indicate the high sensitivity of our 3D tubular microsensor to various ionic species.

Currently, several efforts are ongoing toward single cell detection using microfluidic devices based on label free conductivity measurements. Morgan et al.<sup>45–47</sup> presented interesting works regarding current methods for single cell dielectric spectroscopy, including theoretical studies and simulations. Sun et al.<sup>48</sup> concluded in their theoretical study that for identical geometrical parameters, a design based on parallel electrodes is more sensitive than a coplanar configuration. In this sense, an improved behavior would be expected by using our 3D tubular microsensors.

The high sensitivity of the rolled-up tubular microsensors to solutions of low ionic strength inspires us to explore their bioapplication, such as detection of cancer cells, which is highly important in cancer diagnosis. The presence of various anionic molecules, such as phosphatidylserine,<sup>49</sup> sialic acid, and heparin sulfate<sup>50</sup> on cancer cell membranes lead to an overall negatively charged cell surface in comparison to negligible or weak

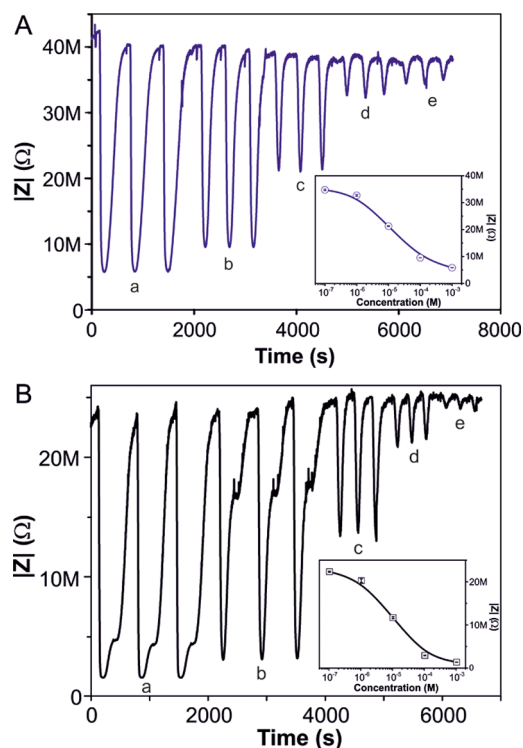


**Figure 3.** Calibration performed with the 3D tubular microsensor for several  $\text{NH}_4\text{Cl}$  (A) and  $\text{CaCl}_2$  (B) concentrations: [a] =  $10^{-3}$  M; [b] =  $10^{-4}$  M; [c] =  $10^{-5}$  M; [d] =  $10^{-6}$  M; and [e] =  $10^{-7}$  M. Flow rate and sample volume were set at  $18 \mu\text{L}/\text{min}$  and  $20 \mu\text{L}/\text{min}$ , respectively, for both salts. A sinusoidal signal with amplitude of 1 V<sub>pp</sub> and frequency equal to 1 and 10 kHz for  $\text{NH}_4\text{Cl}$  and  $\text{CaCl}_2$ , respectively, was applied to measure the solution impedance. Insets show calibration plots obtained for  $\text{NH}_4\text{Cl}$  and  $\text{CaCl}_2$  at different concentrations ( $10^{-3}$ – $10^{-7}$  M) for the tubular microsensor.

negative charged noncancerous cell membranes.<sup>51</sup> The presence of cancer cells may then have an impact on the bulk electrical properties of an aqueous solution with low ionic strength due to the attraction of cations to the vicinity of the cells and the isolative plasma membrane and low mobility of the cells. Indeed, when we flew  $20 \mu\text{L}$   $1\times$  phosphate-buffered saline (PBS) containing HeLa cells through the sensor, we detected an increase in the resistance compared to the baseline of PBS (Figure 4A). Figure 4A shows the real-time monitoring of resistance changes when flowing PBS of different HeLa cell concentrations. The calibration plot (inset in Figure 4A) indicates a linear response with the HeLa cells ranging from 900 to 9000 cells/mL in flowing solutions ( $2 \mu\text{L}/\text{min}$ ) with a detection limit of  $\sim 5$  cells/mL. To our knowledge, no existing electrical system detects suspended cancer cells in flowing solutions at such a low concentration. Furthermore, the sensor was able to respond to a single cell within a nearly one million cells/mL solution. Figure 4B shows the real time variations in the resistance when a single HeLa cell in a  $9 \times 10^5$  cells/mL concentration passes through the tubular cavity of the sensor. We observed a sudden increase in the resistance magnitude of about 20 k $\Omega$  and a sharp return to the baseline, corresponding to the cell passing through the microtube, marked inside yellow circle. We therefore conclude that our rolled-up tubular impedimetric sensor is capable of detecting single cancer cells in flow conditions in a real-time, label-free and nondestructive manner.

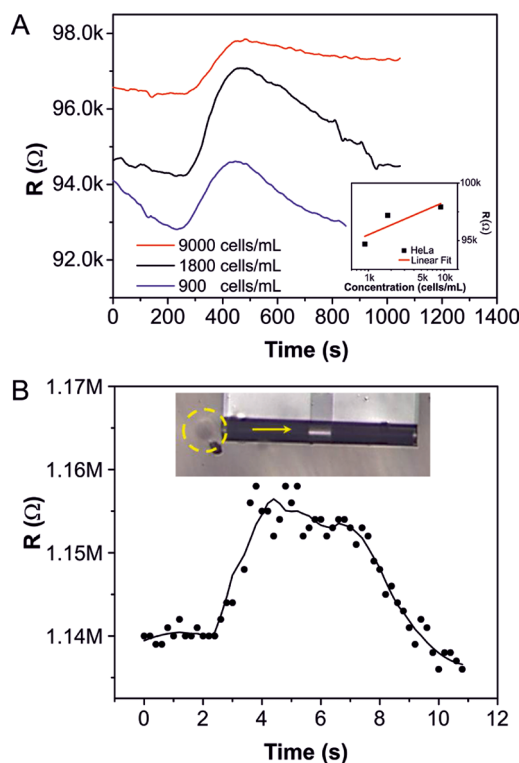


**Figure 4.** Detection of cellular population and single cell events with integrated tubular sensors. (A) Real-time monitoring of the resistance when flowing PBS solutions of varied HeLa cell concentrations through the microchannel. The frequency of the sinusoidal signal applied during measurement was 1 kHz and the voltage was 1 V<sub>pp</sub>. The inset shows the calibration plot of resistance versus cell concentrations and the linear fit to the data. (B) Optical image presents a single HeLa cell (yellow dash cycle, top) is about to go through the tubular cavity of the sensor (yellow arrow indicates the direction) and the corresponding real-time changes in the resistance read-out (bottom).

In this work, we presented the fabrication of a 3D tubular impedimetric microsensors with rolled-up nanotechnology integrated into microfluidic chips. The tubular cavity of the sensor enhances the sensitivity to the impedance of aqueous solutions and allows the label-free detection of various ionic species at significantly low concentrations. Particularly, without functionalization of the sensor surface, we demonstrate its potential to detect suspended cancer cells in flowing PBS down to single cell resolution. In comparison with other cell sensors employing optical or magnetic methods,<sup>25,52–54</sup> our reusable sensor requests no expensive and complicated instrument, when compared with conventional optical detection systems, and utilizes noninvasive dielectric spectroscopy to analyze the samples. It is then of great interest to improve the sensitivity for distinguishing different cells and identifying other biomaterials. Furthermore, the impedance spectroscopy of single cells within the cavity of the sensor may provide 3D resolution of intrinsic cellular activities. Collectively, the 3D tubular impedance biosensor designed here opens up the possibility of developing a highly compact and rapid platform for future bioapplications and disease diagnostics.

## ■ ASSOCIATED CONTENT

### Supporting Information

More details of the fabrication and characterization methods and the materials used. This material is available free of charge via the Internet at <http://pubs.acs.org>.

## ■ AUTHOR INFORMATION

### Corresponding Authors

\*E-mail: [cynthia.cmc@gmail.com](mailto:cynthia.cmc@gmail.com).

\*E-mail: [sanchez@is.mpg.de](mailto:sanchez@is.mpg.de).

\*E-mail: [o.schmidt@ifw-dresden.de](mailto:o.schmidt@ifw-dresden.de).

### Present Address

(S.S. and W.X.) Max Planck Institute for Intelligent Systems, Heisenbergstrasse 3, 70569 Stuttgart, Germany.

### Author Contributions

C.S.M.C., S.S., and O.G.S. conceived the project, C.S.M.C. and W.X. designed the experiments with help from S.S.. S.S. and O.G.S. supervised the study. C.S.M.C. and W.X. performed and analyzed all experiments with help from S.S. C.S.M.C., S.S., and W.X. wrote the manuscript. All authors commented on and/or edited the manuscript and figures. All authors have given approval to the final version of the manuscript.

### Notes

The authors declare no competing financial interest.

## ■ ACKNOWLEDGMENTS

We thank Stefan Baunack for the SEM images, Ronny Engelhard for technical support and Stefan Harazim, Sebastian Seifert, and Martin Bauer for support in the clean room facilities. C.S.M.C. thanks Céline Vervacke and Daniel Grimm for initial discussions. O.G.S. is grateful for fruitful discussions with Yongfeng Mei and Tao Sun regarding the detection concept of the project. The research leading to these results has received funding from the European Research Council under the European Union's Seventh Framework Programme (FP7/2007-2013)/ERC Grant Agreement 311529 and the Volkswagen foundation (no. 86 362).

## ■ REFERENCES

- (1) El-Ali, J.; Sorger, P. K.; Jensen, K. F. *Nature* **2006**, *442*, 403–411.
- (2) Qin, L.; Vermesh, O.; Shi, Q.; Heath, J. R. *Lab Chip* **2009**, *9*, 2016–2020.
- (3) Schumacher, S.; Nestler, J.; Otto, T.; Wegener, M.; Ehrentreich-Foerster, E.; et al. *Lab Chip* **2012**, *12*, 464–473.
- (4) Nie, F.-Q.; Yamada, M.; Kobayashi, J.; Yamato, M.; Kikuchi, A.; et al. *Biomaterials* **2007**, *28*, 4017–4022.
- (5) Yeo, L. Y.; Chang, H.-C.; Chan, P. P. Y.; Friend, J. R. *Small* **2011**, *7*, 12–48.
- (6) Pui-ock, S.; Ruchirawat, M.; Gascoyne, P. *Anal. Chem.* **2008**, *80*, 7727–7734.
- (7) Ibanez-Garcia, N.; Martinez-Cisneros, C. S.; Valdes, F.; Alonso, J. *TrAC, Trends Anal. Chem.* **2008**, *27*, 24–33.
- (8) Martinez-Cisneros, C. S.; Ibanez-Garcia, N.; Valdes, F.; Alonso, J. *Anal. Chem.* **2007**, *79*, 8376–8380.
- (9) O'Toole, M.; Lau, K. T.; Diamond, D. *Talanta* **2005**, *66*, 1340–1344.
- (10) Lau, K. T.; Baldwin, S.; O'Toole, M.; Shepherd, R.; Yerazunis, W. J.; et al. *Anal. Chim. Acta* **2006**, *557*, 111–116.
- (11) Diamond, D.; Lau, K. T.; Brady, S.; Cleary, J. *Talanta* **2008**, *75*, 606–612.
- (12) Vandaveer, W. R.; Pasas-Farmer, S. A.; Fischer, D. J.; Frankenfeld, C. N.; Lunte, S. M. *Electrophoresis* **2004**, *25*, 3528–3549.
- (13) Wang, J. *Electroanalysis* **2005**, *17*, 1133–1140.

- (14) Pumera, M.; Merkoci, A.; Alegret, S. *TrAC, Trends Anal. Chem.* **2006**, *25*, 219–235.
- (15) Andersson, H.; van den Berg, A. *Sens. Actuators, B* **2003**, *92*, 315–325.
- (16) Yi, C. Q.; Li, C. W.; Ji, S. L.; Yang, M. S. *Anal. Chim. Acta* **2006**, *560*, 1–23.
- (17) Pumera, M. *Talanta* **2007**, *74*, 358–364.
- (18) Kuban, P.; Hauser, P. C. *Electrophoresis* **2009**, *30*, 176–188.
- (19) Kuban, P.; Hauser, P. C. *Electrophoresis* **2013**, *34*, 55–69.
- (20) Matysik, F.-M. *Microchim. Acta* **2008**, *160*, 1–14.
- (21) Tomazelli Coltro, W. K.; Lima, R. S.; Segato, T. P.; Carrilho, E.; de Jesus, D. P.; et al. *Anal. Methods* **2012**, *4*, 25–33.
- (22) Lee, C.-Y.; Chen, C. M.; Chang, G.-L.; Lin, C.-H.; Fu, L.-M. *Electrophoresis* **2006**, *27*, 5043–5050.
- (23) Mahabadi, K. A.; Rodriguez, I.; Lim, C. Y.; Maurya, D. K.; Hauser, P. C.; et al. *Electrophoresis* **2010**, *31*, 1063–1070.
- (24) Schmidt, O. G.; Eberl, K. *Nature* **2001**, *410*, 168–168.
- (25) Prinz, V. Y.; Seleznev, V. A.; Gutakovskiy, A. K.; Chehovskiy, A. V.; Preobrazhenskii, V. V.; et al. *Physica E* **2000**, *6*, 828–831.
- (26) Mei, Y.; Huang, G.; Solovev, A. A.; Ureña, E. B.; Mönch, I.; et al. *Adv. Mater.* **2008**, *20*, 4085–4090.
- (27) Smith, E. J.; Xi, W.; Makarov, D.; Mönch, I.; Harazim, S.; et al. *Lab Chip* **2012**, *12*, 1917–1931.
- (28) Mönch, I.; Makarov, D.; Koseva, R.; Baraban, L.; Karnaushenko, D.; et al. *ACS Nano* **2011**, *5*, 7436–7442.
- (29) Solovev, A. A.; Mei, Y.; Bermúdez Ureña, E.; Huang, G.; Schmidt, O. G. *Small* **2009**, *5*, 1688–1692.
- (30) Xi, W.; Solovev, A. A.; Ananth, A. N.; Gracias, D. H.; Sanchez, S.; et al. *Nanoscale* **2013**, *5*, 1294–1297.
- (31) Songmuang, R.; Rastelli, A.; Mendach, S.; Schmidt, O. G. *Appl. Phys. Lett.* **2007**, *90*, 091905.
- (32) Harazim, S. M.; Bolanos Quinones, V. A.; Kiravittaya, S.; Sanchez, S.; Schmidt, O. G. *Lab Chip* **2012**, *12*, 2649–2655.
- (33) Grimm, D.; Bufon, C. C. B.; Deneke, C.; Atkinson, P.; Thurmer, D. J.; et al. *Nano Lett.* **2013**, *13*, 213–218.
- (34) Bof Bufon, C. C.; Gonzalez, J. D. C.; Thurmer, D. J.; Grimm, D.; Bauer, M.; et al. *Nano Lett.* **2010**, *10*, 2506–2510.
- (35) Schumann, J.; Lisunov, K. G.; Escoffier, W.; Raquet, B.; Broto, J. M.; et al. *Nanotechnology* **2012**, *23*, 255701.
- (36) Vervacke, C.; Bof Bufon, C. C.; Thurmer, D. J.; Schmidt, O. G. *RSC Adv* **2014**, *4*, 9723–9729.
- (37) Ji, H.-X.; Wu, X.-L.; Fan, L.-Z.; Krien, C.; Fiering, I.; et al. *Adv. Mater.* **2010**, *22*, 4591–4595.
- (38) Yan, C.; Xi, W.; Si, W.; Deng, J.; Schmidt, O. G. *Adv. Mater.* **2013**, *25*, 539–544.
- (39) Smith, E. J.; Schulze, S.; Kiravittaya, S.; Mei, Y.; Sanchez, S.; et al. *Nano Lett.* **2011**, *11*, 4037–4042.
- (40) Mark, J. J. P.; Coufal, P.; Opekar, F.; Matysik, F.-M. *Anal. Bioanal. Chem.* **2011**, *401*, 1669–1676.
- (41) Kuban, P.; Hauser, P. C. *Electrophoresis* **2004**, *25*, 3387–3397.
- (42) Kuban, P.; Hauser, P. C. *Electrophoresis* **2004**, *25*, 3398–3405.
- (43) Boynton, A. L.; Whitfield, J. F. *Proc. Natl. Acad. Sci. U.S.A.* **1976**, *73*, 1651–1654.
- (44) Durham, A. C. H.; Walton, J. M. *Biosci. Rep.* **1982**, *2*, 15–30.
- (45) Morgan, H.; Sun, T.; Holmes, D.; Gawad, S.; Green, N. G. *J. Phys. D: Appl. Phys.* **2007**, *40*, 61.
- (46) Gawad, S.; Sun, T.; Green, N. G.; Morgan, H. *Rev. Sci. Instrum.* **2007**, *78*, 054301.
- (47) Sun, T.; Gawad, S.; Bernabini, C.; Green, N. G.; Morgan, H. *Meas. Sci. Technol.* **2007**, *18*, 2859.
- (48) Sun, T.; Green, N. G.; Gawad, S.; Morgan, H. *IET Nanobiotechnol.* **2007**, *1*, 69–79.
- (49) Riedl, S.; Zweytick, D.; Lohner, K. *Chem. Phys. Lipids* **2011**, *164*, 766–781.
- (50) Ang, I. L.; Poon, T. C. W.; Lai, P. B. S.; Chan, A. T. C.; Ngai, S.-M.; et al. *J. Proteome Res.* **2006**, *5*, 2691–2700.
- (51) Bevers, E. M.; Comfurius, P.; Zwaal, R. F. A. *Lupus* **1996**, *5*, 480–487.
- (52) Huang, H.-T.; Ger, T.-R.; Lin, Y.-H.; Wei, Z.-H. *Lab Chip* **2013**, *13*, 3098–3104.
- (53) Ger, T.-R.; Huang, H.-T.; Huang, C.-Y.; Lai, M.-F. *Lab Chip* **2013**, *13*, 4225–4230.
- (54) Moosung, K.; Hwang, D. J.; Jeon, H.; Hiromatsu, K.; Grigoropoulos, C. P. *Lab Chip* **2009**, *9*, 311–18.